Alteration of birnessite reactivity in dynamic anoxic/oxic environments

Qinzhi Li [a], Dieter Schild [b], Mathieu Pasturel [c], Johannes Lützenkirchen [b], Khalil Hanna [a,d,*]

[a] Univ Rennes, École Nationale Supérieure de Chimie de Rennes, CNRS, ISCR – UMR6226, F-35000 Rennes, France
[b] Institute for Nuclear Waste Disposal (INE), Karlsruhe Institute of Technology (KIT), P.O. 3640, D-76021 Karlsruhe, Germany
[c] Univ. Rennes, CNRS, ISCR – UMR 6226, F-35000 Rennes, France
[d] Institut Universitaire de France (IUF), MESRI, 1 rue Descartes, 75231 Paris, France

HIGHLIGHTS

- Birnessite reactivity was highly sensitive to variable redox condition.
- Surface-catalyzed oxidation of Mn(II) enabled formation of reactive Mn(III) sites.
- Increase in Mn(II)/MnO_2 molar ratio suppressed MnO_2 reactivity.
- Reactivity enhancement was observed in dynamic two-step anoxic/oxic process.
- Oscillating redox conditions in environmental settings may affect contaminant fate.

GRAPHICAL ABSTRACT

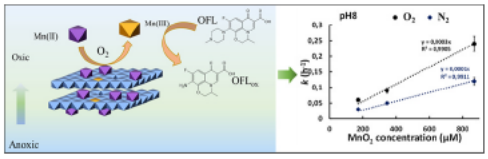

ARTICLE INFO

Editor: Baiyang Chen

Keywords:
Manganese oxide
Redox
Antibiotics
Oxidation
Removal

ABSTRACT

Although the oxidative capacity of manganese oxides has been widely investigated, potential changes of the surface reactivity in dynamic anoxic/oxic environments have been often overlooked. In this study, we showed that the reactivity of layer structured manganese oxide (birnessite) was highly sensitive to variable redox conditions within environmentally relevant ranges of pH (4.0 – 8.0), ionic strength (0–100 mM NaCl) and Mn(II)/MnO_2 molar ratio (0–0.58) using ofloxacine (OFL), a typical antibiotic, as a target contaminant. In oxic conditions, OFL removal was enhanced relative to anoxic environments under alkaline conditions. Surface-catalyzed oxidation of Mn(II) enabled the formation of more reactive Mn(III) sites for OFL oxidation. However, an increase in Mn(II)/MnO_2 molar ratio suppressed MnO_2 reactivity, probably because of competitive binding between Mn (II) and OFL and/or modification in MnO_2 surface charge. Monovalent cations (*e.g.*, Na^+) may compensate the charge deficiency caused by the presence of Mn(III), and affect the aggregation of MnO_2 particles, particularly under oxic conditions. An enhancement in the removal efficiency of OFL was then confirmed in the dynamic two-step anoxic/oxic process, which emulates oscillating redox conditions in environmental settings. These findings call for a thorough examination of the reactivity changes at environmental mineral surfaces (*e.g.*, MnO_2) in natural systems that may be subjected to alternation between anaerobic and oxygenated conditions.

1. Introduction

Manganese dioxides (MnO_2) are ubiquitous in a wide range of aquatic and terrestrial environments (Post, 1999). They are widely used in various energy and environmental applications, because of their specific nanoscale properties, high surface areas, low cost, strong

* Corresponding author at: Univ Rennes, École Nationale Supérieure de Chimie de Rennes, CNRS, ISCR – UMR6226, F-35000 Rennes, France.
E-mail address: khalil.hanna@ensc-rennes.fr (K. Hanna).

oxidation and sorption abilities (Post, 1999; Remucal and Ginder-Vogel, 2014). The layer structured manganese oxide (*e.g.,* birnessite) is structurally similar to biogenically precipitated natural manganese oxides, and thus the common natural occurring MnO_2 in surficial environments. It basically consists of randomly stacked edge-sharing MnO_6 octahedra and has a large excess of negative charges because of the Mn(IV) vacancies and substitution of Mn(II)/(III) for Mn(IV) (Elzinga, 2011). As a result, MnO_2 exhibits a high affinity for cation sorption, but also a non-negligible anion adsorption capacity. Another important feature of MnO_2 is the ease of switching the oxidation state, which imparts a good catalytic activity (Post, 1999; Remucal and Ginder-Vogel, 2014).

In oxic environments, it has been reported that MnO_2 surfaces can catalyze the oxidation of Mn(II) by dissolved oxygen to generate Mn (III)/(IV) (Yang et al., 2018; Zhao et al., 2016), while homogeneous oxidation of Mn(II) by oxygen is considered kinetically sluggish (Davies and James, 1989; Diem and Stumm, 1984; Lan et al., 2017; Nico et al., 2002; Wilson, 1980). Surface oxygen ligands bound to inner-sphere adsorbed Mn(II) may accelerate the electron transfer between Mn(II) and O_2 (Junta and Hochella, 1994; Lan et al., 2017; Luther, 2005; Namgung et al., 2020), leading to higher Mn(II) removal under oxic conditions compared to anoxic conditions at circumneutral to alkaline pH (Elzinga, 2011; Lefkowitz et al., 2013; Li et al., 2020). The accumulated Mn(III) can incorporate into Mn octahedral layers and induce the transformation of MnO_2 (Hinkle et al., 2017; Wang et al., 2018a).

Although the influence of phase transformation on the reactivity of birnessite has been already investigated (Lefkowitz and Elzinga, 2015; Wang et al., 2018a, 2019), very little knowledge exists about the impact of oxygen on the removal of organic compounds interacting with MnO_2 surfaces. Furthermore, MnO_2 may co-exist with dissolved Mn(II) and emerging contaminants in natural systems which may be subjected to alternation between anaerobic and oxic conditions, such as water-sediment interfaces, water table fluctuations, groundwater recharge (Jeong et al., 2010; Wu et al., 2020; Zhao et al., 2021). However, little is known about the potential changes in the surface reactivity of MnO_2 in environmental settings under alternating redox conditions. This work has examined for the first time how a shift of redox conditions from anoxic into oxic may alter the reactivity of birnessite.

Ofloxacin (OFL) was chosen here as a target contaminant in order to explore the changes in MnO_2 reactivity under dynamic anoxic/oxic conditions. OFL is widely used in human and veterinary medicine, and frequently detected in surface water, groundwater, soils and municipal wastewater systems, with concentration ranging from ng/L to μg/L (Zhang and Huang, 2005). Removal kinetics of OFL in the presence of acid birnessite were investigated at pH ranging from 4.0 to 8.0, representing the common pH conditions of suboxic environments (Elzinga, 2016; Wang et al., 2018a). The oxidation byproducts of OFL were determined using an ultra performance liquid chromatography-tandem mass spectrometry (UPLC-MS/MS). The oxidative capacity of MnO_2 was further monitored for variable Mn(II)/MnO_2 molar ratios and ionic strengths under environmentally relevant conditions. In addition, X-ray diffraction (XRD), X-ray photoelectron spectroscopy (XPS) and scanning electron microscopy (SEM) were used to identify the changes in Mn valence states and mineral phase transformation. This work calls for more consideration of alteration of the oxidative capacity of birnessite in redox transition zone in groundwater systems.

2. Materials and Methods

2.1. Materials and Chemicals

All chemicals employed in this study were purchased from Sigma-Aldrich of analytical grade and used without further purification. Ultrapure water (specific resistivity, 18.2 MΩ cm^{-1}, Milli-Q, Millipore) was used for all solutions and suspensions.

Acid birnessite was synthesized by reacting $KMnO_4$ and HCl as described in previous studies (Li et al., 2020; Mckenzie, 1971; Pokharel et al., 2020). The purity of mineral phase was confirmed with XRD and SEM (Fig. S1). The specific surface area (SSA) measured by Brunauer-Emmett-Teller (BET)-N_2 adsorption was 85.0 ± 3.0 m^2 g^{-1} and the isoelectric point (pH_{IEP}) was around 2.0, respectively (Fig. S2). Analysis of XPS data showed that the average oxidation state of the pristine material was 3.87, with 88.3% Mn(IV), 10.7% Mn(III) and 1.0% Mn(II) (Fig. S3).

2.2. Batch experiments

All batch experiments were carried out in 500 mL polyethylene bottles, containing varying concentrations of acid birnessite. The solutions were spiked with aliquots of 1.0 mM OFL and 0.05 M $MnCl_2$ stock solution to achieve initial concentration of 10 μM OFL and variable target Mn(II) concentrations ranging from 0 to 200 μM. The ionic strength was fixed using NaCl at various concentrations. The pH of the suspensions was adjusted to the desired values over the reaction time using an auto pH titrator with addition of small volumes of HCl (0.1 M) or NaOH (0.1 M) solutions and maintained at pH 4.0, 6.0 and 8.0 throughout the experiments. No pH buffers were used, to prevent any impact on the birnessite reactivity. The stirring speed of the mixture was maintained at 350 rpm. Batch experiments were carried out under ambient air atmosphere or by bubbling oxygen gas (oxic conditions), or by bubbling nitrogen gas (anoxic conditions). A two-step anoxic/oxic dynamic process was investigated as follows: after a period of anoxic conditions where the bottle was under N_2, an oxic environment was subsequently created by removing the cap of the bottle or by bubbling O_2. The same kinetic behavior was observed when either the suspension was stirred under open atmosphere (ambient air) or with bubbling O_2 (data not shown). In the open system, CO_2 from the atmosphere will generate carbonates in solution at high pH values, but this effect on the reactivity can be excluded according to a previous study (Li et al., 2020).

Aliquots of solution were periodically withdrawn and filtered through a 0.20 μm membrane filter for analysis of OFL concentration, whereas other aliquots without filtration were immediately mixed with 0.1 M ascorbic acid to quench the reaction. At the end of experiments, the remaining suspensions were centrifuged at 4500 rpm for 20 min and settled particles were freeze-dried, and then stored at 4 ℃ for further solid analysis. In another experimental series involving mixing with 1.0 mM sodium pyrophosphate, a volume of about 3.0 mL sample was periodically withdrawn from the mixed solution, filtered and analyzed immediately by UV Vis spectrophotometry in the range of 200–600 nm wavelength. Batch experiments were conducted in triplicates and the standard deviation was calculated for each experimental series.

2.3. Analytical methods

The concentration of OFL in the samples was analyzed via High Performance Liquid Chromatography analysis with UV Vis detection (HPLC-UV) equipped with a reversed-phase C18 column (250 mm × 4.6 mm i.d., 5 μm) and a UV Vis detector (Waters 2489) at a wavelength of 287 nm. The mobile phase consisted of acetonitrile/water (15/85 v/v,) containing 0.1% formic acid at a flow rate of 0.6 mL/min.

Filtered suspensions were digested with 2% nitric acid and dissolved Mn(II) concentrations were determined by Atomic Absorption Spectroscopy (AAS, AA140, Varian, Shimadzu) with a detection limit of 0.02 μM.

The oxidation byproducts of OFL were identified using an ultra performance liquid chromatography-tandem mass spectrometry (UPLC-MS/MS) system. An electrospray interface was used for the MS measurements in positive ionisation mode and full scan acquisition.

XPS spectra were recorded on an XPS system PHI 5000 VersaProbe II (ULVAC-PHI Inc.) equipped with a scanning microprobe X-ray source (monochromatic Al Kα, hν 1486.7 eV). An electron flood gun generating low energy electrons (1.1 eV) and low energy argon ions (6 eV) by a floating ion gun were applied for charge compensation at isolating

samples (dual beam technique). Survey scans were recorded with an X-ray source power of 31 W, X-ray spot size diameter 200 μm, and pass energy of the analyzer of 187.85 eV. Narrow scans of the elemental lines were recorded at 23.5 eV pass energy, which yields an energy resolution of 0.69 eV FWHM at the Ag $3d_{5/2}$ elemental line of pure silver. Calibration of the binding energy scale of the spectrometer was performed using well-established binding energies of elemental lines of pure metals (monochromatic Al Kα: Cu $2p_{3/2}$ at 932.62 eV, Au 4 $f_{7/2}$ at 83.96 eV) (Seah et al., 1998). The error in binding energies of elemental lines is estimated to ± 0.1 eV for conductors and ± 0.2 eV for isolating samples. High-resolution XPS spectra were calibrated by the carbon deposit C1s binding energy at 284.8 eV and further analyzed by CasaXPS software. After Shirley background subtractions, all peaks were fitted using 70:30 Gaussian: Lorentzian sum function.

A FEI Quanta 650 FEG environmental scanning electron microscope (now Thermo Fisher Scientific Inc.) was applied to image the sample surfaces.

XRD data were collected by using a D8 Advance (Bruker) diffractometer with Cu Kα radiation over the range of 10–80° 2θ at a step size of 0.02° and phases were determined according to the PDF database in Jade 6 software.

3. Results and Discussion

3.1. Effect of oxygen and pH on the initial removal rate of OFL by MnO_2

Removal kinetics of OFL were investigated under anoxic and oxic conditions as a function of MnO_2 concentration (173–870 μM or 15 75.6 mg/L) at three pH values (4.0, 6.0, 8.0 (± 0.1)) over 8 h of reaction time (Fig. S4). The entire kinetic curve could not be properly described by simple equations that include classical exponential functions (*e.g.,* first- or second- order model), probably due to the complexity of involved reactions including accumulation and competition of reaction products (*e.g.* OFL byproducts, Mn(II) ions, etc.) and/or a gradual change of the reactivity of surface sites. For the sake of simplicity and to overcome possible interference caused by the accumulated byproducts, we have determined the rate constant over the first stage of reaction (*i.e.,* 1 h). The initial rate constants k (h^{-1}) calculated by linear regression of ln [OFL] /$[OFL]_o$ versus time, were plotted against MnO_2 concentration in Fig. 1. The correlation coefficients (R^2) of linear regression (ln C /C_o -kt) were above 0.90 for all experiments.

The rate constants exhibited the same order, pH 4.0 > pH 6.0 > pH 8.0, regardless of MnO_2 concentration. This is consistent with previous reports (Li et al., 2020; Zhang and Huang, 2005; Zhang et al., 2008), which showed that acidic conditions enabled higher quinolones removal in the presence of MnO_2. This can be ascribed to more favorable interactions between the less negatively charged surface (pH_{IEP} of MnO_2 ~ 2.0) and OFL (pK_a 6.08 and 8.25, Fig. S5) at acidic pH values. Furthermore, the decrease in redox potential of MnO_2 from 0.99 V to 0.76 V when the pH increased from 4.0 to 8.0 would also explain the enhanced reactivity under acidic conditions, as previously reported (Li et al., 2020).

Mass balance showed that adsorption and oxidation are involved in the removal of OFL in the presence of MnO_2, even though the adsorption appears to be relatively weak for our experimental conditions (*e.g.,* less than 1.5 μmol m^{-2}, at pH 6.0; less than 0.1 μmol m^{-2}, at pH 8.0). Based on previous investigations for fluoroquinolones (Kamagate et al., 2019; Martin et al., 2015; Zhou et al., 2019), OFL may form metal-bonded complexes with surface sites and/or directly hydrogen-bonded complexes with surface hydroxo groups involving both carboxylate and keto groups. However, accurate quantification of the adsorption is not straightforward, because binding of redox-active compounds to birnessite is followed by an electron transfer process resulting in the concomitant oxidation of sorbed compound and reduction of surface-bound metal. LC/MS analysis showed that OFL oxidation passes through partial or full N-dealkylation of the piperazine ring, as two predominant products of m/z 336 (M-26) and m/z 279 (M-69) have been detected (See Fig. S6 for more details). Indeed, the piperazine ring of OFL can be oxidized through two one-electron transfers from the N atom of piperazine ring to Mn(IV), and then N-dealkylation and/or C-hydroxylation causes ring opening, as typically observed for similar compounds (Zhang and Huang, 2005). Additionally, trace amounts of

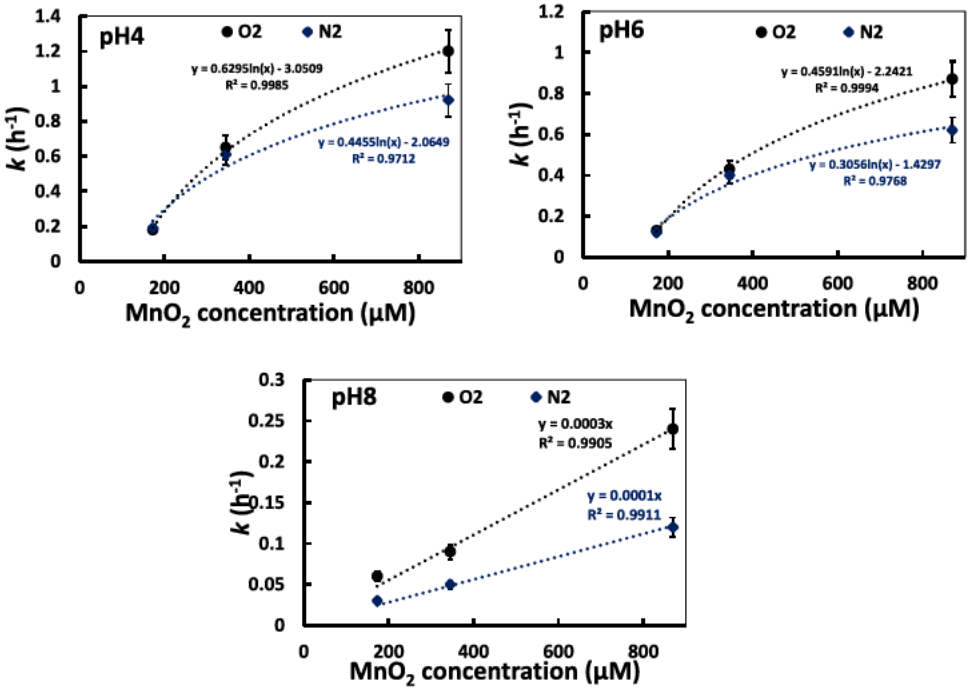

Fig. 1. Initial removal rate constants of OFL *versus* MnO_2 concentration at three pH values 4.0, 6.0, 8.0 (± 0.1). 173, 345, 870 μM (15, 30, 75.6 mg/L) MnO_2; 10 μM OFL; 10 mM NaCl; under anoxic (N_2) and oxic (O_2) conditions. Dashed lines are the best correlation obtained between k and MnO_2 amount. Correlation coefficients (R^2) are indicators of the strength of the linear or non-linear relationship.

M+ 16, M-44 (decarboxylation), M-101 and M+ 30 were detected, as previously reported for the Mn-based oxidation of OFL (Li et al., 2021; Zhang and Huang, 2005).

The effect of oxygen on the removal efficiency of OFL was only observed at high MnO_2 concentration (870 μM) or at pH 8.0 ± 0.1 for the full range of MnO_2 concentration (Fig. 1). In both conditions, the apparent pseudo-first-order rate constant k (h^{-1}) increased with increasing MnO_2 concentration. It is worth noting that a linear dependence of reactivity on MnO_2 amount was only observed at pH 8.0, while a logarithmic relationship was observed at pH 4.0 and 6.0 (Fig. 1). Contribution of Fenton-like reaction through, for instance hydroxyl radical formation, in OFL removal is excluded, since the addition of ethanol, used as a hydroxyl radical scavenger, has no effect on the OFL removal (Fig. S7). Furthermore, we found that the impact of oxygen on birnessite reactivity at pH 8.0 is not specific to OFL, since similar behavior has been observed with another antibiotic compound, pipemidic acid (see Fig. S8).

It is generally known that the reaction of MnO_2 with redox-active compounds is complex and involves several reaction pathways that occur simultaneously. The redox byproducts generated through reductive dissolution of MnO_2 or OFL oxidation, can bind onto the MnO_2 surfaces, and alter the initial surface reactivity (*i.e.,* passivation). Generally, the generated Mn(II) is sorbed onto the MnO_2 surface and then oxidized. Mn(IV) is reduced, and the resulting product is Mn(III), which is commonly called the comproportionation reaction (Wang et al., 2019; Zhao et al., 2016). In addition, the adsorbed Mn(II) on vacant sites can be oxidized by O_2 at high pH to yield Mn(III). Because higher MnO_2 concentration enables more OFL oxidation (higher k, Fig. 1), more reductive dissolution or Mn(II) production is expected. Dissolved Mn(II) was below the detection limit (< 0.02 μM for AAS) in all investigated conditions, confirming that generated Mn(II) by reductive dissolution of MnO_2 was completely removed by binding to MnO_2. Competitive binding between OFL and Mn(II) at MnO_2 edge sites, and/or adsorption of OFL oxidation byproducts at the MnO_2 surface may also explain the passivation of the Mn-oxide surface. All these reactions are pH-dependent, as well as the passivation of MnO_2 surfaces. This may explain why the relationship between the oxidation rate constant of OFL and MnO_2 content is not linear over the whole pH range investigated (Fig. 1). Furthermore, higher surface-oxidation rates of Mn(II) at alkaline pH values (Lefkowitz et al., 2013; Namgung et al., 2014) may explain the pronounced impact of oxygen on birnessite reactivity at pH 8.0 (Fig. 1).

Collectively, these results suggest that enhanced removal efficiency of OFL under oxic conditions at high MnO_2 concentration or high pH is due to the Mn(III) generated through Mn(II) surface-catalyzed oxidation by oxygen. This is, however, in disagreement with a recent work which reported that oxygen inhibited phenol degradation by δ-MnO_2 because the generated Mn(III)-phases at the MnO_2 surface may block reactive sites and cause particle aggregation, thereby lowering the surface reactivity (Hu et al., 2019). This discrepancy with the present work may be explained by the difference in experimental conditions including target contaminant characteristics and its affinity to MnO_2 surfaces, and target compound/MnO_2 molar ratio.

On the other hand, previous works have reported that the Mn(III) oxides or Mn(III) complexes can rapidly oxidize a variety of organic compounds (Chen et al., 2013; Huang et al., 2018; Klewicki and Morgan, 1999; Nico and Zasoski, 2001). Mn(III) is a strong oxidant for one electron transfer reaction (Hu et al., 2017; Sun et al., 2021), compared to two electron transfer reaction involving Mn(IV).

$$Mn\ (III) + e^- \rightarrow Mn\ (II)\ E^0 \quad +1.51\ V \tag{1}$$

$$Mn(III)OOH + 3\ H^+ + e^- \rightarrow Mn\ (II) + 2\ H_2O\ E^0 \quad +1.50\ V \tag{2}$$

$$Mn(IV)O_2 + 4\ H^+ + 2e^- \rightarrow Mn\ (II) + H_2O\ E^0 \quad +1.29\ V \tag{3}$$

In a heterogeneous system, the greater reactivity of Mn(III)-bearing phases has been explained by longer and weaker Mn(III)-O bonds facilitating the electron transfer with sorbing compounds (*e.g.,* phenol) (Huang et al., 2018; Ukrainczyk and McBride, 1992). It seems that direct coordination of Mn(III) with target compounds ensures to facilitate electron transfer without change in the Mn spin state, while the outer sphere electron transfer in surface Mn(IV) requires a change in the Mn spin state, in turn making the electron transfer process more difficult (Huang et al., 2018; Ukrainczyk and McBride, 1992). Indeed, Mn(III) was reported to be as a high spin d^4 ion with much lower ligand field stabilization energy and faster ligand exchange rates comparing with Mn (IV) (Nico and Zasoski, 2000). In contrast, other reports showed that Mn (III) sites are less reactive with respect to target contaminants. For example, lower As(III) oxidation have been attributed to the lower affinity of Mn(III) sites for As(III) adsorption, and slower electron transfer rates with adsorbed As(III) (Lafferty et al., 2010a, 2010b; Zhu et al., 2009). Moreover, the surface functional groups on Mn(III) sites are more labile than functional groups on Mn(IV) sites (Zhu et al., 2009), and therefore stronger adsorption via ligand exchange processes on Mn(III) sites than on Mn(IV) sites is expected. Finally, different types of Mn sites, *e.g.,* Mn(III, IV) in sheets, Mn(III, IV) at edges, and Mn(III) in interlayers, likely have varying reactivity (Manceau et al., 1997; Simanova and Pena, 2015; Yu et al., 2012). The interlayer Mn(III) was suggested to be the dominant oxidizing site, and the abundance of Mn(III) with respect to total Mn may be key in promoting the reactivity of birnessite (Peng et al., 2017). From a kinetic point of view, Mn(III) at the edges seems to contribute at short reaction times, while Mn(III, IV) in the MnO_2 sheets is important at longer times (Simanova and Pena, 2015; Wang et al., 2018b). Despite this conflicting information about the role of structural Mn(III) in promoting MnO_2 reactivity, we may conclude that multiple factors may control the contribution of Mn(III) in enhancing the removal capacity of birnessite. This may include the ratio of Mn(III) to Mn(IV), mineral phase transformation along the redox reaction, and properties of target contaminants and its interaction with Mn sites. To gain more insights into the underlying passivation mechanisms, the effects of Mn (II)/MnO_2 ratio on the removal kinetics of OFL were investigated under oxic and anoxic conditions in the following Section.

3.2. *Combined effects of Mn(II) and O_2 under a wide range of ionic strength*

As an attempt to confirm the impact of surface-catalyzed oxidation of Mn(II) by O_2 on the reactivity of MnO_2, OFL removal kinetics were investigated with different Mn(II)/MnO_2 molar ratios at pH 8.0 (Fig. 2). As expected, the initial rate constants of OFL sharply decreased with increasing Mn(II) under both investigated conditions. As previously reported (Chen et al., 2010; Li et al., 2020; Remucal and Ginder-Vogel, 2014), dissolved Mn(II) strongly adsorbed on the negatively charged birnessite surfaces, resulting in competition between OFL and Mn(II) binding to the reactive surface sites of MnO_2. This Mn(II) binding is much more important at alkaline pH values (Lefkowitz et al., 2013). The adsorbed Mn(II) on vacant sites at high pH is oxidized to Mn(III) through surface-catalyzed oxidation of Mn(II) enabling more Mn(III) in the vacancies (Zhu et al., 2010). This explains why the dissolved Mn(II) concentration was found here below the AAS detection limit, even for the highest Mn(II) amount (200 μM). Time-dependent UV-Vis measurements for birnessite suspensions containing 200 μM Mn(II), suggested more generated Mn(III) in the presence of oxygen relative to anoxic conditions (Fig. S9). Indeed, the intensity of adsorption bands at 258 nm for the potential Mn(III)-PP complex (λ_1 480 nm, ε_1 65 M^{-1}; λ_2 258 nm, ε_2 6750 M^{-1}) (Hu et al., 2017) was found to be higher under oxic conditions.

It should be noted that the greater reactivity of birnessite under oxic conditions relative to anoxic systems is only observed at lower Mn(II)/MnO_2 molar ratio (≤ 0.1). At higher ratio, strong competition between Mn(II) and OFL may act as a counterweight to the Mn(III) contribution, thereby reducing the overall reactivity of MnO_2.

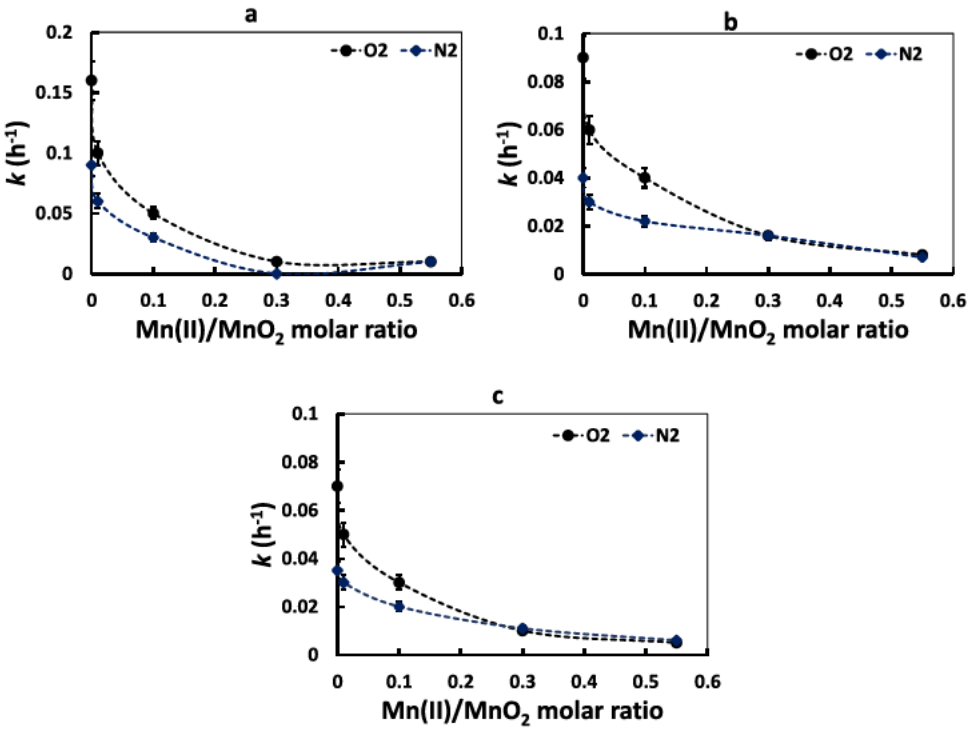

Fig. 2. Initial removal rate constants of OFL as a function of Mn(II)/MnO_2 molar ratio under anoxic or oxic conditions. pH 8.0 (± 0.1), 345 μM (30 mg/L) acid birnessite. 0, 5, 50, 100, 200 μM Mn(II); 10 μM OFL; (a) 0 mM NaCl, (b) 10 mM NaCl, (c) 100 mM NaCl. Dashed lines are only as visual guide.

When removal kinetics was investigated at higher ionic strength (10 or 100 mM of NaCl), a decrease in the initial rate constants of OFL was observed, mainly under oxic conditions and at low Mn(II)/MnO_2 molar ratio (Fig. 2). Increasing ionic strength may increase the size of MnO_2 via oriented aggregations (Burrows et al., 2012; Yang et al., 2019), thereby reducing the surface reactivity. This decrease in surface reactivity has also been previously observed during aging of manganese oxides through coalescence of particles (Stone and Morgan, 1984). Furthermore, Na^+ ions may compete with the cationic Mn(II) and/or zwitterionic form of OFL ($pK_{a,1}$ 6.08 and $pK_{a,2}$ 8.25) for negatively charged adsorptive sites on MnO_2 (pH_{IEP} ~ 2.0). Na^+ can occupy the interlayers of birnessite, potentially competing with Mn(II) and/or influencing the diffusion process of Mn(II) at reactive surface sites (Yang et al., 2019). Previous work reported similar competitive binding due to the presence of monovalent or divalent cations, resulting in a decrease in the rate and magnitude of organic compound transformation (Chen et al., 2010). Under oxic conditions, oxidation of Mn(II) into Mn(III) and subsequent incorporation of Mn(III) into the layers may occur, resulting in birnessite transformation from hexagonal to orthogonal layer symmetry (Zhao et al., 2016). In this case, Na^+ ions could compensate for the charge deficiency caused by the presence of Mn(III), and subsequently act to stabilize Mn(III) in the layers (Drits et al., 2007; Zhu et al., 2010). This may explain the pronounced effect of increasing NaCl concentration on the MnO_2 surface reactivity in the presence of O_2.

To check whether transition zones at oxic-anoxic interfaces may influence the reactivity of birnessite, removal kinetics experiments were conducted for 24 h under N_2, with subsequent ambient air conditions or bubbling O_2 for 48 h (Fig. 3). Under anoxic conditions, a plateau was observed at around 16 h, and then continued over 72 h. When suspensions were exposed to ambient air or O_2 after a pre-equilibration period of 24 h under N_2, OFL was further removed up to 65%, which could be ascribed to the Mn(III) generated through Mn(II) surface-catalyzed oxidation by oxygen. As mentioned above, these newly generated Mn (III) are more reactive for OFL oxidation. It should be noted that strong oxygenation of solution with bubbling O_2 has no greater effect on the birnessite reactivity, as compared to the solution exposed to ambient air.

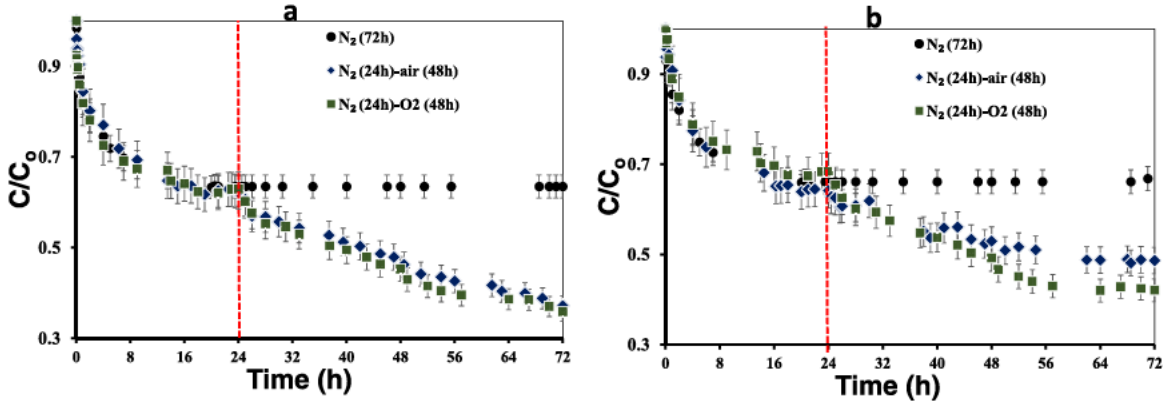

Fig. 3. Removal kinetics of OFL in dynamic same two-step anoxic/oxic process: (a) 0 μM Mn(II); (b) 5 μM Mn(II). pH 8.0 (± 0.1); 10 μM OFL; 10 mM NaCl; 345 μM acid birnessite. The red vertical line indicates the beginning of oxygenation through exposure to ambient air or with bubbling O_2.

The same two-step anoxic/oxic process was repeated but in the presence of 5 μM Mn(II). This Mn(II) amount was chosen to cover the typical range of Mn concentration found in surface and groundwaters (~ 4 μM) (Namgung et al., 2014). The presence of 5 μM Mn(II) did not significantly affect the removal rate whether under oxic or anoxic conditions. Only a slight inhibition was observed especially for longer reaction times, likely because of competitive effects of Mn(II) and OFL for binding onto reactive sites. In all conditions, removal kinetic exhibited a plateau under N_2, followed by a drop in the aqueous concentration of OFL when the reaction medium was exposed to air or O_2 (Fig. 3).

3.3. XRD and XPS investigations

To evaluate the role of Mn speciation on reactivity changes and the passivation of the MnO_2 surface, XPS analysis of initial and reacted MnO_2 samples were performed under defined experimental conditions.

First, the total contents of major elements are reported in Table S1. In the absence of Mn(II), a decrease in Mn content in reacted samples was observed, likely resulting from the presence of various adsorbing ligands at the surface (Table S1) (Shaikh et al., 2016). Higher Na content under oxic conditions also proved the compensation effect of Na^+ as discussed above. Increasing Mn(II) concentrations from 50 μM to 200 μM enhanced Mn percentage, likely because of the adsorption of Mn(II) onto the MnO_2 surfaces. K content was below detection limit, likely due to the large adsorption amounts of Mn exchanging with interlayer K^+ ion.

Second, the high resolution spectra of Mn $2p_{3/2}$ was then fitted and the BE (binding energy) positions of Mn(II), Mn(III), Mn(IV) ranged from 640.1 to 641.4 eV, from 642.1 to 642.4 eV and from 642.6 to 643.1 eV, respectively, consistent with previously reported values (Fig. 4, Table S2) (Sun et al., 2019; Tang et al., 2013, 2014). We have subsequently determined the average oxidation state (AOS) of all samples, and found that the AOS (initial value 3.87) decreased for all reacted samples (Table S2).

As expected, increasing the Mn(II) concentration from 0 μM to 200 μM enhanced the amount of Mn(II) bond to MnO_2 surfaces (Fig. 4). An increase in the percentage of Mn(III) was also observed in the presence of oxygen relative to anoxic conditions, while that of Mn(IV) decreased. As previously explained, Mn(II) can undergo surface-catalyzed oxidation by molecular oxygen and/or comproportionation with structural Mn(IV) forming Mn(III) sites. Both processes can enhance the Mn(III) content in MnO_2, particularly under oxic conditions (Table S2).

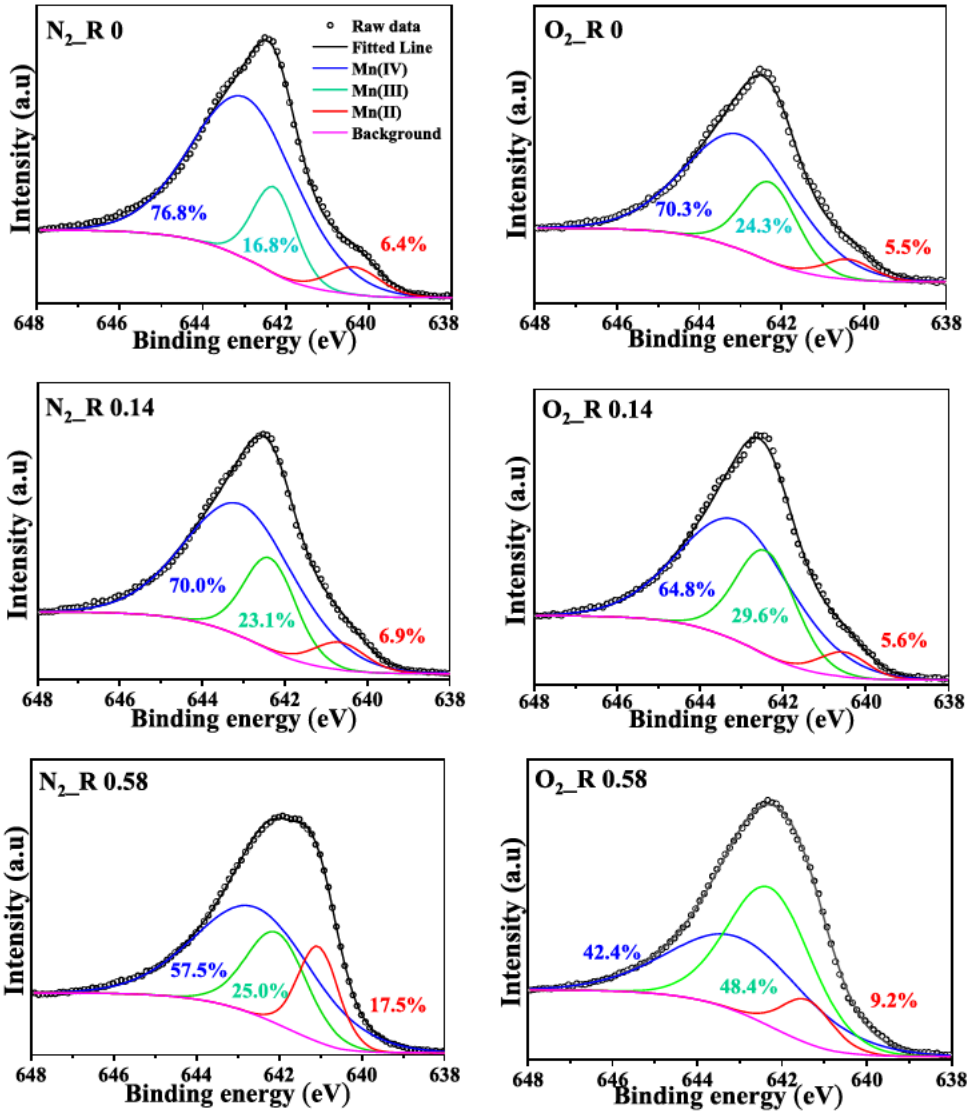

Fig. 4. Fitting of Mn $2p_{3/2}$ XPS high resolution spectra of the synthesized pristine acid birnessite and samples treated with Mn(II) and OFL under anoxic and oxic conditions. The R represents the Mn(II)/MnO_2 molar ratio. 345 μM acid birnessite; 10 μM OFL; 10 mM NaCl; 0, 50, 200 μM Mn(II); 48 h reaction time; pH 8.0 (± 0.1). The numbers inset are the percentage of Mn(II) (red), Mn(III) (green) and Mn(IV) (blue).

The high-resolution spectra of O1s were then evaluated to assess potential transformation of birnessite surfaces (Table S3 and Fig. S10). The compositions of oxygen bonding types consisted of a main peak located at around 530.2 eV corresponding to lattice oxygen with metal (O_{latt}), a shoulder peak near 531.6 eV attributing to the adsorbed oxygen species on MnO_2 surface (O_{ads}) in the form of hydroxide oxygen (OH^-) and the weakest peak at higher binding energy assigning to the adsorbed oxygen in water molecule (O_{surf}) (Tang et al., 2013; Zhang et al., 2020). After reaction, the increased proportions of H_2O suggested that the surface became progressively hydroxylated and hydrated. It is worth noting that in the presence of 200 μM Mn(II), high contents in Mn(III) and OH^- under anoxic condition have been considered as characteristic of intermediate reaction products Mn(III)-hydroxide, here represented as MnOOH (Nesbitt et al., 1998). Moreover, the content of O_{latt} decreased to 49% (anoxic) and 65% (oxic), which suggests that lattice oxygen may participate in the oxidation of Mn(II) with the formation of oxygen vacancy (Cheng et al., 2019). Once the O_{latt} is consumed, dissolved oxygen could compensate (Cheng et al., 2019), which would explain the difference in O_{latt} content between anoxic and oxic environments.

The produced Mn(III) may incorporate into the layer of birnessite and induce the changes of mineral structure by converting birnessite into lower valence Mn phases (Zhao et al., 2016). To check possible phase transformation, XRD analysis of MnO_2 samples under various Mn (II)/MnO_2 molar ratios (R) and under anoxic and oxic conditions was conducted (Fig. 5). Samples reacted with OFL in the presence of dissolved Mn(II) (50 μM, R 0.14) showed no bulk transformation. However, XRD data of samples with higher R (i.e. 0.29 or 0.58) showed different peaks, both under anoxic and oxic conditions, which could suggest the presence of lower valence Mn oxides, e.g. feitknechite (β-MnOOH) (Wang et al., 2018a; Lefkowitz et al., 2013). This is consistent with SEM images where needle-shaped particles were observed amid nanoflower-shaped particles of birnessite, especially at higher Mn(II) concentration and under oxic conditions (Fig. S11). These needle-shaped crystals can be attributed either to the presence of manganite (γ-MnOOH) as previously reported by *e.g.* Larsen et al. (1998), or more certainly according to XRD data, to feitknechtite as previously reported by Lefkowitz et al. (2013).

4. Conclusions

As a result of natural or anthropogenic activities, such as groundwater recharge, sediment dredging, water table fluctuations, etc., alternating redox conditions commonly occur in natural systems. Here, we have demonstrated for the first time that the oxygen can alter the redox reactivity of MnO_2 under environmentally-relevant conditions of Mn(II) dosage, pH and ionic strength. A decline in the oxidation rate constant with increasing pH was observed, likely because of the decrease in the redox potential of MnO_2 at higher pH and modification in surface interactions with the target compound. At high pH, the adsorbed Mn(II) on vacant sites can be oxidized by O_2 or Mn(IV) surrounding the vacant sites into Mn(III) (comproportionation reaction). Therefore, OFL adsorbed at vacant sites can be oxidized by the newly generated Mn(III) sites, which seems to be strong oxidizing species. However, excess dissolved Mn(II) would compete with compounds for binding at reactive sites, thus decreasing the removal capacity of birnessite. The decreased reactivity of MnO_2 with higher ionic strength also suggested that the sorption of alkali cation (Na^+) on the surface may affect the birnessite reactivity. Furthermore, sequential anoxic-oxic dynamic process may significantly impact the fate of existing contaminants in the presence of birnessite. Combining anoxic and oxic environments into one process may be relevant in many subsurface environments, for instance, when anoxic aquifers and/or sediments come into contact with oxygen. Further redox oscillation studies are needed to explore the fate and mobility of contaminants and co-existing natural compounds (*e.g.*, dissolved organic matter), in the presence of manganese oxides.

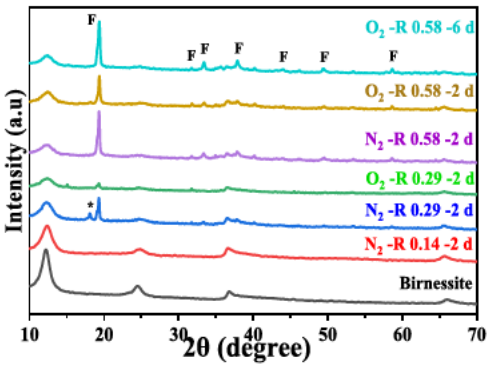

Fig. 5. XRD patterns of the MnO_2 samples treated with Mn(II) and OFL under oxic and anoxic conditions. 345 μM acid birnessite; 10 μM OFL; 10 mM NaCl; 0, 50, 100, 200 μM Mn(II); 48 h or 6 d reaction time; pH 8.0 (± 0.1). The R represents the Mn(II)/MnO_2 molar ratio. The f symbols indicate XRD peaks visible on the feitknechtite (β-MnOOH) sample in Lefkowitz et al. (2013); the * symbol has previously been attributed to hausmannite (Wang et al., 2018a) but in the absence of the main Bragg peaks of this phase, it would rather belong to an hydrated α-MnO_2 phase (Rossouw et al., 1992).

CRediT authorship contribution statement

KH and JL designed the study. QL carried out the experiments and wrote the original draft. DS and MP performed the solid characterizations. KH, QL and JL wrote, reviewed and edited the manuscript. All authors discussed the results and commented on the manuscript.

Declaration of Competing Interest

The authors declare that they have no known competing financial interests or personal relationships that could have appeared to influence the work reported in this paper.

Acknowledgments

K.H thanks the Institut Universitaire de France (IUF 2017-2022) for support, Q.L thanks the Chinese Scholarship Council of PR China (2018-2021) for her Ph.D. grant and Rennes Métropole (France, RM2021) for a mobility grant for an extended research visit at KIT (Germany). We want to acknowledge Valerie Courousse (AAS) and Kouhail Yasmine (XRD) for providing help in experiments.

Appendix A. Supporting information

Supplementary data associated with this article can be found in the online version at doi:10.1016/j.jhazmat.2022.128739.

References

Burrows, N.D., Hale, C.R.H., Penn, R.L., 2012. Effect of ionic strength on the kinetics of crystal growth by oriented aggregation. Cryst. Growth Des. 12, 4787–4797.
Chen, W., Ding, Y., Johnston, C.T., Teppen, B.J., Boyd, S.A., Li, H., 2010. Reaction of lincosamide antibiotics with manganese oxide in aqueous solution. Environ. Sci. Technol. 44, 4486–4492.
Chen, W.R., Liu, C., Boyd, S.A., Teppen, B.J., Li, H., 2013. Reduction of carbadox mediated by reaction of Mn(III) with oxalic acid. Environ. Sci. Technol. 47, 1357–1364.
Cheng, Y., Huang, T., Liu, C., Zhang, S., 2019. Effects of dissolved oxygen on the start-up of manganese oxides filter for catalytic oxidative removal of manganese from groundwater. Chem. Eng. J. 371, 88–95.
Davies, S.H.R., James M., J., 1989. Manganese(II) oxidation kinetics on metal oxide surfaces. J. Colloid Interface Sci. 129, 63–77.
Diem, D., Stumm, W., 1984. Is dissolved Mn^{2+} being oxidized by O_2 in absence of Mn-bacteria or surface catalysts? Geochim. Cosmochim. Acta 48, 1571–1573.
Drits, V.A., Lanson, B., Gaillot, A., 2007. Birnessite polytype systematics and identification by powder X-ray diffraction. Am. Mineral. 92, 771–788.
Elzinga, E.J., 2011. Reductive transformation of birnessite by aqueous Mn(II). Environ. Sci. Technol. 45, 6366–6372.

Elzinga, E.J., 2016. 54Mn radiotracers demonstrate continuous dissolution and reprecipitation of vernadite (δ-MnO2) during interaction with aqueous Mn (II). Environ. Sci. Technol. 50, 8670–8677.
Hinkle, M.A.G., Orcid, K.G.D., Catalano, J.G., 2017. Impact of Mn(II)-manganese oxide reactions on Ni and Zn speciation. Environ. Sci. Technol. 51, 3187–3196.
Hu, E., Zhang, Y., Wu, S., Wu, J., Liang, L., He, F., 2017. Role of dissolved Mn(III) in transformation of organic contaminants: Non-oxidative versus oxidative mechanisms. Water Res. 111, 234–243.
Hu, E., Pan, S., Zhang, W., Zhao, X., Liao, B., He, F., 2019. Impact of dissolved O_2 on phenol oxidation by δ-MnO_2. Environ. Sci. Process. Impacts 21, 2118–2127.
Huang, J., Zhong, S., Dai, Y., Liu, C., Zhang, H., 2018. Effect of MnO_2 phase structure on the oxidative reactivity toward bisphenol A degradation. Environ. Sci. Technol. 52, 11309–11318.
Jeong, H.Y., Han, Y., Park, S.W., Hayes, K.F., 2010. Aerobic oxidation of mackinawite (FeS) and its environmental implication for arsenic mobilization. Geochim. Cosmochim. Acta 74, 3182–3198.
Junta, J.L., Hochella Jr., M.F., 1994. Manganese (II) oxidation at mineral surfaces: a microscopic and spectroscopic study. Geochim. Cosmochim. Acta 58, 4985–4999.
Kamagate, M., Pasturel, M., Brigante, M., Hanna, K., 2019. Mineralization enhancement of pharmaceutical contaminants by radical-based oxidation promoted by oxide-bound metal ions. Environ. Sci. Technol. 54, 476–485.
Klewicki, J., Morgan, J., 1999. Dissolution of β-MnOOH particles by ligands: pyrophosphate, ethylenediaminetetraacetate, and citrate. Geochim. Cosmochim. Acta 63, 3017–3024.
Lafferty, B.J., Ginder-Vogel, M., Sparks, D.L., 2010a. Arsenite oxidation by a poorly crystalline manganese-oxide 1. Stirred-flow experiments. Environ. Sci. Technol. 44, 8460–8466.
Lafferty, B.J., Ginder-Vogel, M., Zhu, M., Livi, K.J.T., Sparks, D.L., 2010b. Arsenite oxidation by a poorly crystalline manganese-oxide. 2. Results from X-ray absorption spectroscopy and X-ray diffraction. Environ. Sci. Technol. 44, 8467–8472.
Lan, S., Wang, X., Xiang, Q., Yin, H., Tan, W., Qiu, G., Liu, F., Zhang, J., Feng, X., 2017. Mechanisms of Mn(II) catalytic oxidation on ferrihydrite surfaces and the formation of manganese (oxyhydr)oxides. Geochim. Cosmochim. Acta 211, 79–96.
Larsen, I., Little, B., Nealson, K.H., Ray, R., Stone, A., Tian, J., 1998. Manganite reduction by Shewanella putrefaciens MR-4. Am. Mineral. 83, 1564–1572.
Lefkowitz, J.P., Elzinga, E.J., 2015. Impacts of aqueous Mn(II) on the sorption of Zn(II) by hexagonal birnessite. Environ. Sci. Technol. 49, 4886–4893.
Lefkowitz, J.P., Rouff, A.A., Elzinga, E.J., 2013. Influence of pH on the reductive transformation of birnessite by aqueous Mn(II). Environ. Sci. Technol. 47, 10364–10371.
Li, K., Xu, A., Wu, D., Zhao, S., Meng, T., Zhang, Y., 2021. Degradation of ofloxacin by a manganese-oxidizing bacterium Pseudomonas sp. F2 and its biogenic manganese oxides. Bioresour. Technol. 328, 124826.
Li, Q., Pokharel, R., Zhou, L., Pasturel, M., Hanna, K., 2020. Coupled effects of Mn(II), pH and anionic ligands on the reactivity of nanostructured birnessite. Environ. Sci. Nano 7, 4022–4031.
Luther, G.W., 2005. Manganese(II) oxidation and Mn(IV) reduction in the environment-two one-electron transfer steps versus a single two-electron step. Geomicrobiol. J. 22, 195–203.
Manceau, A., Silvester, E., Bartoli, C., Lanson, B., Drits, V.A., 1997. Structural mechanism of Co^{2+} oxidation by the phyllomanganate buserite. Am. Mineral. 82, 1150–1175.
Martin, S., Shchukarev, A., Hanna, K., Boily, J., 2015. Kinetics and mechanisms of ciprofloxacin oxidation on hematite surfaces. Environ. Sci. Technol. 49, 12197–12205.
Mckenzie, R.M., 1971. The synthesis of birnessite, cryptomelane, and some other oxides and hydroxides of manganese. Mineral. Mag. 38, 493–502.
Namgung, S., Kwon, M.J., Qafoku, N.P., Lee, G., 2014. $Cr(OH)_3$ (s) oxidation induced by surface catalyzed Mn(II) oxidation. Environ. Sci. Technol. 48, 10760–10768.
Namgung, S., Guo, B., Sasaki, K., Lee, S.S., Lee, G., 2020. Macroscopic and microscopic behaviors of Mn(II) (ad)sorption to goethite with the effects of dissolved carbonates under anoxic conditions. Geochim. Cosmochim. Acta 277, 300–319.
Nesbitt, H.W., Canning, G.W., Bancroft, G.M., 1998. XPS study of reductive dissolution of 7Å-birnessite by H3AsO3, with constraints on reaction mechanism. Geochim. Cosmochim. Acta 62, 2097–2110.
Nico, P.S., Zasoski, R.J., 2000. Importance of Mn (III) availability on the rate of Cr(III) oxidation on δ-MnO_2. Environ. Sci. Technol. 34, 3363–3367.
Nico, P.S., Zasoski, R.J., 2001. Mn (III) center availability as a rate controlling factor in the oxidation of phenol and sulfide on δ-MnO_2. Environ. Sci. Technol. 35, 3338–3343.
Nico, P.S., Anastasio, C., Zasoski, R.J., 2002. Rapid photo-oxidation of Mn(II) mediated by humic substances. Geochim. Cosmochim. Acta 66, 4047–4056.
Peng, H., McKendry, I.G., Ding, R., Thenuwara, A.C., Kang, Q., Shumlas, S.L., Strongin, D.R., Zdillab, M.J., Perdew, J.P., 2017. Redox properties of birnessite from a defect perspective. Proc. Natl. Acad. Sci. U.S.A. 114, 9523–9528.
Pokharel, R., Li, Q., Zhou, L., Hanna, K., 2020. Water flow and dissolved MnII alter transformation of pipemidic acid by manganese oxide. Environ. Sci. Technol. 54, 8051–8060.
Post, J.E., 1999. Manganese oxide minerals: crystal structures and economic and environmental significance. Proc. Natl. Acad. Sci. U.S.A. 96, 3447–3454.
Remucal, C.K., Ginder-Vogel, M., 2014. A critical review of the reactivity of manganese oxides with organic contaminants. Environ. Sci. Process. Impacts 16, 1247–1266.
Rossouw, M.H., Liles, D.C., Thackeray, M.M., David, W.I.F., Hull, S., 1992. Alpha manganese dioxide for lithium batteries: a structural and electrochemical study. Mat. Res. Bull. 27, 221–230.
Seah, M.P., Gilmore, I.S., Beamson, G., 1998. XPS: binding energy calibration of electron spectrometers 5ÈRe-evaluation of the reference energies. Surf. Interface Anal. 26, 642–649.
Shaikh, N., Taujale, S., Zhang, H., Artyushkova, K., Ali, A.S., Cerrato, J.M., 2016. Spectroscopic investigation of interfacial interaction of manganese oxide with triclosan, aniline, and phenol. Environ. Sci. Technol. 50, 10978–10987.
Simanova, A.A., Pena, J., 2015. Time-resolved investigation of cobalt oxidation by Mn (III)-Rich δ-MnO_2 using quick X-ray absorption spectroscopy. Environ. Sci. Technol. 49, 10867–10876.
Stone, A.T., Morgan, J.J., 1984. Reduction and dissolution of manganese(III) and manganese(IV) oxides by organics. 1. Reaction with hydroquinone. Environ. Sci. Technol. 18, 450–456.
Sun, Q., Cui, P., Liu, C., Peng, S., Alves, M.E., Zhou, D., Shi, Z., Wang, Y., 2019. Antimony oxidation and sorption behavior on birnessites with different properties (δ-MnO2 and triclinic birnessite). Environ. Pollut. 246, 990–998.
Sun, Y., Im, J., Shobnam, N., Fanourakis, S.K., He, L., Anovitz, L.M., Erickson, P.R., Sun, H., Zhuang, J., Loffler, F.E., 2021. Degradation of adsorbed bisphenol A by soluble Mn(III). Environ. Sci. Technol. 55, 13014–13023.
Tang, Q., Jiang, L., Liu, J., Wang, S., Sun, G., 2013. Effect of surface manganese valence of manganese oxides on the activity of the oxygen reduction reaction in alkaline media. ACS Catal. 4, 457–463.
Tang, W., Wu, X., Li, D., Wang, Z., Liu, G., Liu, H., Chen, Y., 2014. Oxalate route for promoting activity of manganese oxide catalysts in total VOCs'oxidation: effect of calcination temperature and preparation method. J. Mater. Chem. A 2, 2544–2554.
Ukrainczyk, L., McBride, M.B., 1992. Oxidation of phenol in acidic aqueous suspensions of manganese oxides. Clays Clay Min. 40, 157–166.
Wang, Q., Yang, P., Zhu, M., 2018a. Structural transformation of birnessite by fulvic acid under anoxic conditions. Environ. Sci. Technol. 52, 1844–1853.
Wang, Q., Yang, P., Zhu, M., 2019. Effects of metal cations on coupled birnessite structural transformation and natural organic matter adsorption and oxidation. Geochim. Cosmochim. Acta 250, 292–310.
Wang, Y., Benkaddour, S., Marafatto, F.F., Pena, J., 2018b. Diffusion- and pH-dependent reactivity of layer-type MnO_2: reactions at particle edges versus vacancy sites. Environ. Sci. Technol. 52, 3476–3485.
Wilson, D.E., 1980. Surface and complexation effects on the rate of Mn(II) oxidation in natural waters. Geochim. Cosmochim. Acta 44, 1311–1371.
Wu, J., Zhao, J., Hou, J., Xing, B., 2020. The fate of p-nitrophenol in goethite-rich and sulfide-containing dynamic anoxic/oxic environments. Environ. Sci. Technol. 54, 9427–9436.
Yang, P., Lee, S., Post, J.E., Xu, H., Wang, Q., Xu, W., Zhu, M., 2018. Trivalent manganese on vacancies triggers rapid transformation of layered to tunneled manganese oxides (TMOs): implications for occurrence of TMOs in low-temperature environment. Geochim. Cosmochim. Acta 240, 173–190.
Yang, P., Post, J.E., Wang, Q., Xu, W., Geiss, R., McCurdy, P.R., Zhu, M., 2019. Metal adsorption controls stability of layered manganese oxides. Environ. Sci. Technol. 53, 7453–7462.
Yu, Q., Sasaki, K., Tanaka, K., Ohnuki, T., Hirajima, T., 2012. Structural factors of biogenic birnessite produced by fungus Paraconiothyrium sp. WL-2 strain affecting sorption of Co^{2+}. Chem. Geol. 310–311, 106–113.
Zhang, H., Huang, C., 2005. Oxidative transformation of fluoroquinolone antibacterial agents and structurally related amines by manganese oxide. Environ. Sci. Technol. 39, 4474–4483.
Zhang, H., Chen, W., Huang, C., 2008. Kinetic modeling of oxidation of antibacterial agents by manganese oxide. Environ. Sci. Technol. 42, 5548–5554.
Zhang, H., Xu, F., Xue, J., Chen, S., Wang, J., Yang, Y., 2020. Enhanced removal of heavy metal ions from aqueous solution using manganese dioxide-loaded biochar: Behavior and mechanism. Sci. Rep. 10, 1–13.
Zhao, H., Zhu, M., Li, W., Elzinga, E.J., Villalobos, M., Liu, F., Zhang, J., Feng, X., Sparks, D.L., 2016. Redox reactions between Mn(II) and hexagonal birnessite change its layer symmetry. Environ. Sci. Technol. 50, 1750–1758.
Zhao, J., Su, A., Tian, P., Tang, X., Collins, R.N., He, F., 2021. Arsenic (III) removal by mechanochemically sulfidated microscale zero valent iron under anoxic and oxic conditions. Water Res. 198, 117132.
Zhou, L., Martin, S., Cheng, W., Lassabatere, L., Boily, J., Hanna, K., 2019. Water flow variability affects adsorption and oxidation of ciprofloxacin onto hematite. Environ. Sci. Technol. 53, 10102–10109.
Zhu, M., Paul, K.W., Kubicki, J.D., Sparks, D.L., 2009. Quantum chemical study of arsenic (III, V) adsorption on mn-oxides: implications for arsenic(III) oxidation. Environ. Sci. Technol. 43, 6655–6661.
Zhu, M., Ginder-Vogel, M., Parikh, S.J., Feng, X., Sparks, D.L., 2010. Cation effects on the layer structure of biogenic Mn-oxides. Environ. Sci. Technol. 44, 4465–4471.

Supporting information

Alteration of Birnessite Reactivity in Dynamic Anoxic/Oxic Environments

Qinzhi Li[a], Dieter Schild[b], Mathieu Pasturel[c], Johannes Lützenkirchen[b] and Khalil Hanna[a,d,*]

[a]*Univ Rennes, École Nationale Supérieure de Chimie de Rennes, CNRS, ISCR – UMR6226, F-35000 Rennes, France*

[b]*Institute for Nuclear Waste Disposal (INE), Karlsruhe Institute of Technology (KIT), P.O. Box 3640, D-76021 Karlsruhe, Germany.*

[c]*Univ. Rennes, CNRS, ISCR – UMR 6226, F-35000, Rennes, France*

[d]*Institut Universitaire de France (IUF), MESRI, 1 rue Descartes, 75231 Paris, France.*

[*]Corresponding author: K Hanna, +33 2 23 23 80 27; khalil.hanna@ensc-rennes.fr

Table S1. Atomic concentrations by XPS survey scans for pristine birnessite and samples after reacted with OFL and different Mn(II) concentrations. 345 μM acid birnessite; 10 μM OFL; 10 mM NaCl; 0, 50, 200 μM Mn(II); 48 h reaction time; pH 8 (± 0.1).

	C (%)	O (%)	Mn (%)	K (%)	N (%)	Na (%)
Acid birnessite	27.3	44.9	20.9	6.9	BDL	BDL
N_2_0μM Mn(II)	27.6	44.6	20.4	7.0	0.5	BDL
O_2_0μM Mn(II)	24.3	43.3	17.5	6.1	BDL	8.7
N_2_50μM Mn(II)	21.3	49.5	23.1	5.4	BDL	0.7
O_2_50μM Mn(II)	24.6	44.6	24.6	6.2	BDL	BDL
N_2_200μM Mn(II)	20.9	52.6	26.5	BDL	BDL	BDL
O_2_200μM Mn(II)	21.2	50.5	28.3	BDL	BDL	BDL

BDL: below the detection limit (0.1%).

Table S2. Mn $2p_{3/2}$ XPS fitted parameters for pristine birnessite and samples after reacted with OFL and different Mn(II) concentrations. 345 μM acid birnessite; 10 μM OFL; 10 mM NaCl; 0, 50, 200 μM Mn(II); 48 h reaction time; pH 8 (± 0.1).

Sample		Acid birnessite	0μM Mn(II) N_2	0μM Mn(II) O_2	50μM Mn(II) N_2	50μM Mn(II) O_2	200μM Mn(II) N_2	200μM Mn(II) O_2
AOS		3.87	3.70	3.65	3.63	3.60	3.40	3.33
Mn(II)	Binding energy (eV)	640 1	640.3	640.4	640.7	640.9	641.1	641.4
	Area (%)	1.0	6.4	5.5	6 9	5.6	17.5	9.2
Mn(III)	Binding energy (eV)	642.4	642.3	642.3	642.4	642.4	642.1	642.3
	Area (%)	10.7	16.8	24.3	23.1	29.6	25.0	48.4
Mn(IV)	Binding energy (eV)	643.0	643.0	643.0	643.1	643.1	642.6	643.0
	Area (%)	88.3	76.8	70.2	70.0	64.8	57.5	42.4

Table S3. O 1s XPS fitted parameters for pristine birnessite and samples after reacted with OFL and different Mn(II) concentrations. 345 µM acid birnessite; 10 µM OFL; 10 mM NaCl; 0, 50, 200 µM Mn(II); 48h reaction time; pH 8 (± 0.1).

Sample		Acid birnessite	0µM Mn(II) N_2	0µM Mn(II) O_2	50µM Mn(II) N_2	50µM Mn(II) O_2	200µM Mn(II) N_2	200µM Mn(II) O_2
O_{latt}	Binding energy (eV)	530.2	530.1	530.0	530 1	530.1	529.8	530.0
	Area (%)	87.5	88.5	90.1	88.4	87.3	49.5	65.2
O_{ads}	Binding energy (eV)	531.7	531.5	531.5	531 5	531.6	531.0	531.1
	Area (%)	10.0	8.3	7.0	8.7	9.0	37.8	26.9
O_{surf}	Binding energy (eV)	532.7	532.6	532.7	532.6	532.6	531.9	532.2
	Area (%)	2 5	3.2	2 9	2.9	3.7	12.7	7.9

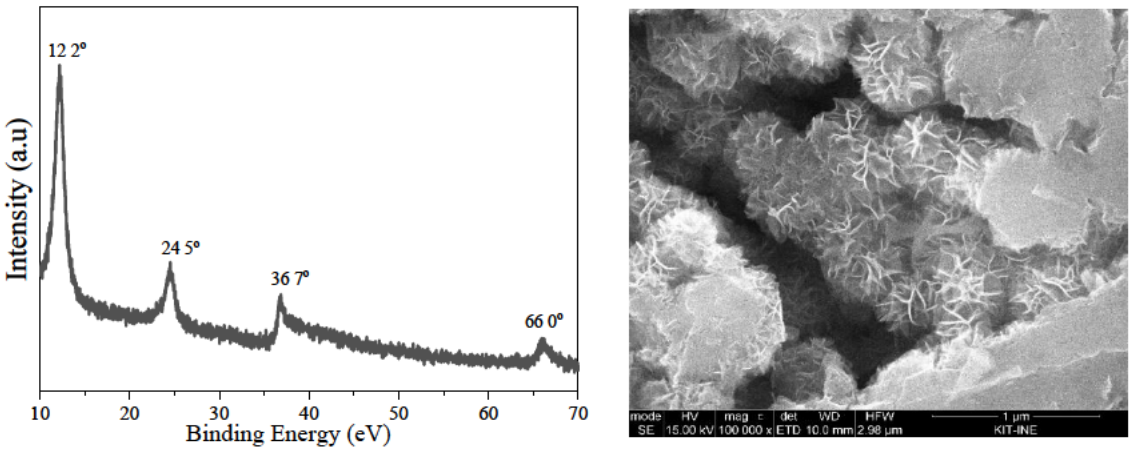

Figure S1. XRD and SEM images of the synthesized birnessite.

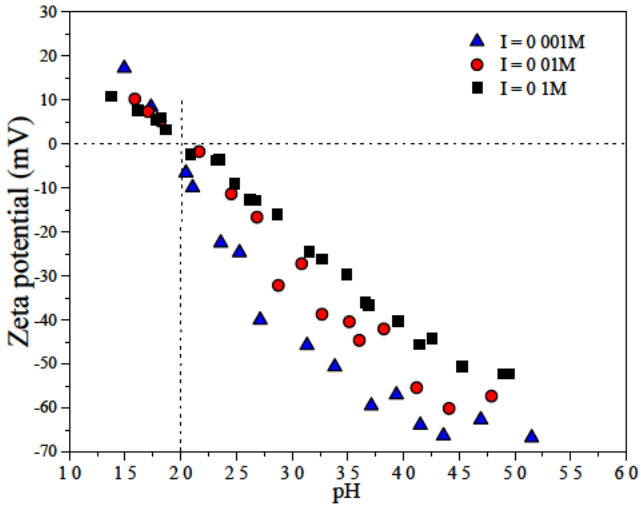

Figure S2. Zeta potential of acid birnessite samples. MnO_2 = 0.2 g L^{-1} (2.3 mM); I = 0.1, 0.01, 0.001 M NaCl.

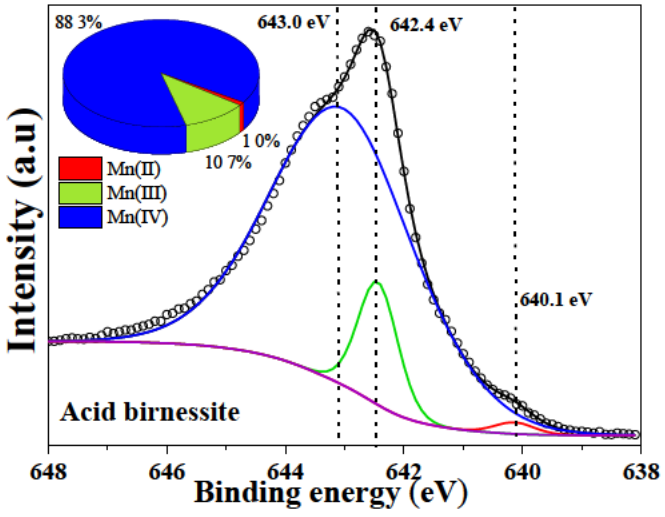

Figure S3. Fitting of Mn $2p_{3/2}$ XPS high resolution spectra of the synthesized acid birnessite.

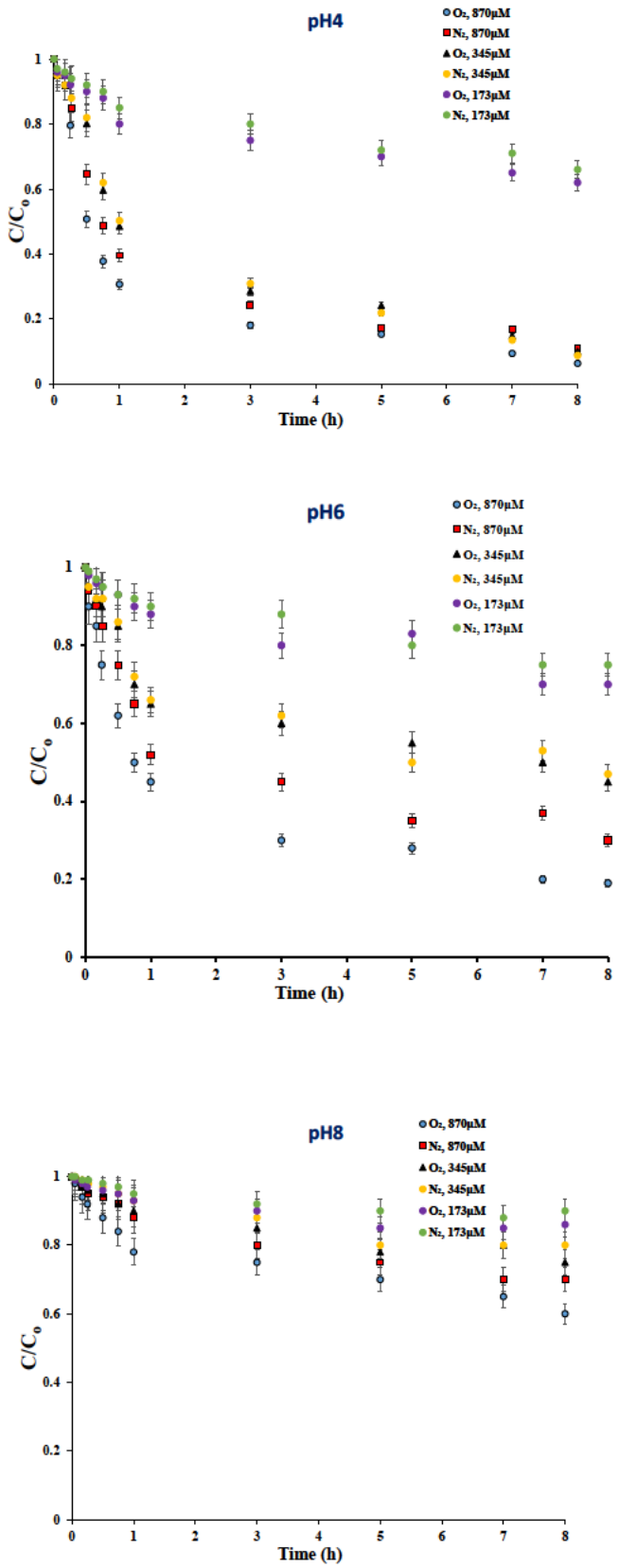

Figure S4. Removal kinetics of OFL at three pH values 4.0, 6.0, 8.0 (± 0.1), and three MnO_2 concentration: 173, 345, 870 μM (or 15, 30, 75.6 mg/L); 10 μM OFL; 10 mM NaCl; under anoxic (N_2) and oxic (O_2) conditions.

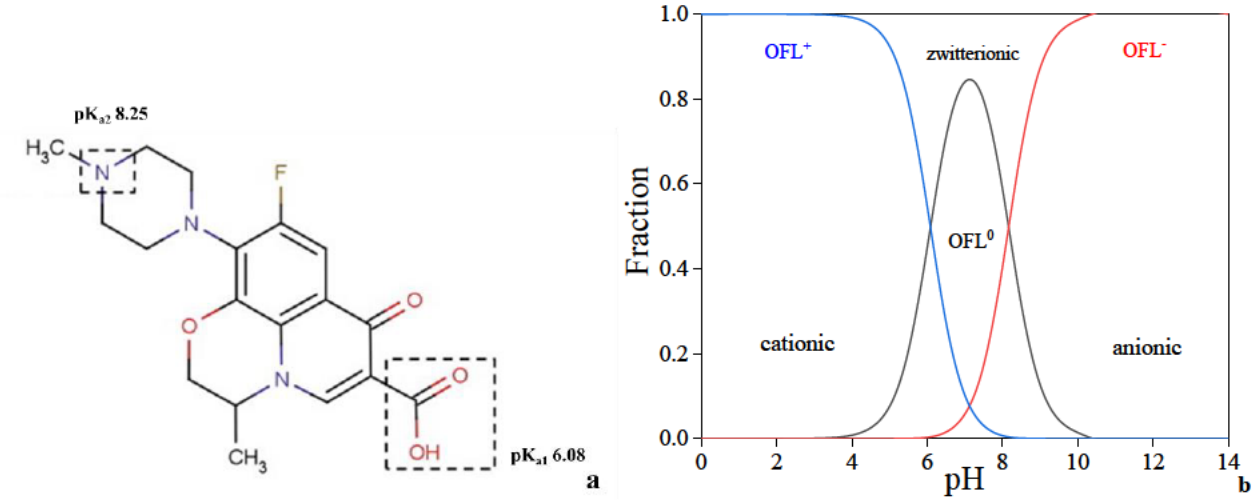

Figure S5. (a) Chemical speciation of OFL *vs* pH. (b) pK_{as} of OFL ($pK_{a,1}$ = 6.08 and $pK_{a,2}$ = 8.25) at infinite dilution were obtained from conditional pK_a values and the Davies equation. 10 mM NaCl.

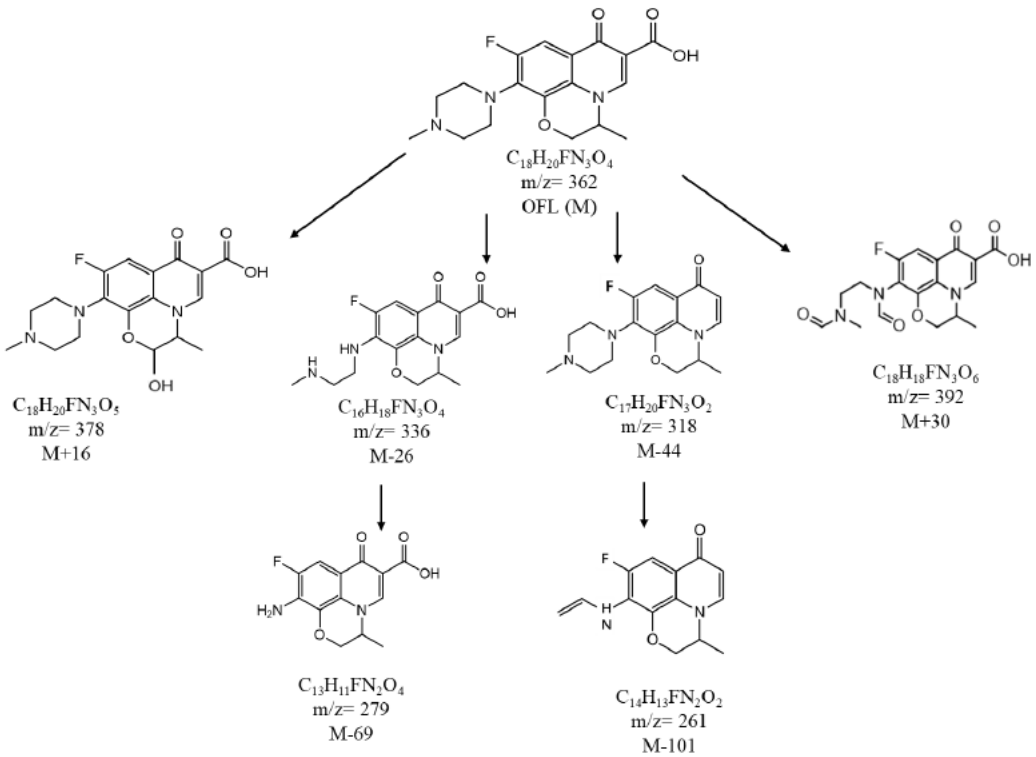

Figure S6. Proposed oxidation pathway of OFL as analyzed by LC/MS. Product of m/z = 279 was classified as the M-69 because of its structural similarity to the M-69 product of CIP (Zhang and Huang, 2005).

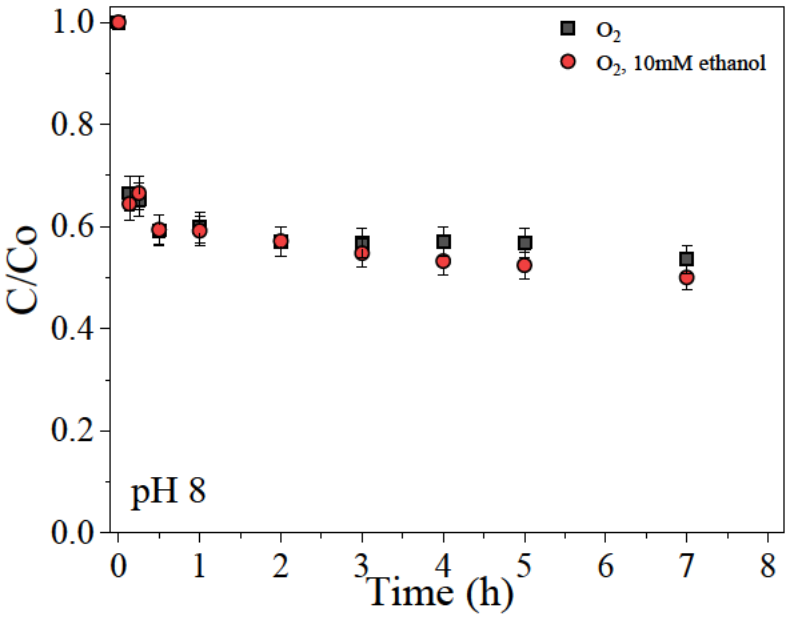

Figure S7. Removal kinetics of OFL in the presence of oxygen and ethanol at pH 8 (± 0.1). 345 µM acid birnessite; 10 µM OFL; 10 mM NaCl; 10 mM ethanol.

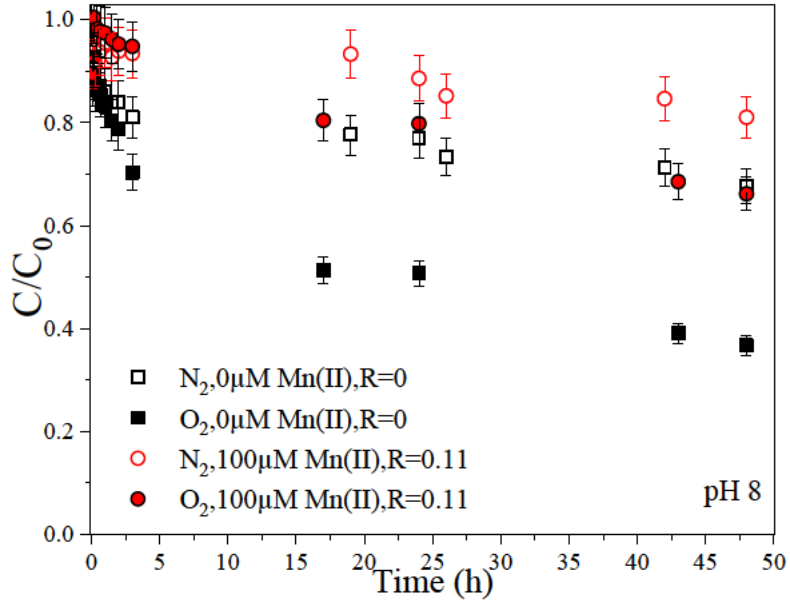

Figure S8. Removal kinetics of pipemidic acid (PIP) under oxic and anoxic conditions at pH 8 (± 0.1). 20 µM PIP; 870 µM acid birnessite; 10 mM NaCl; 0,100 µM Mn(II); 48 h. The R represents the Mn(II)/MnO_2 molar ratio.

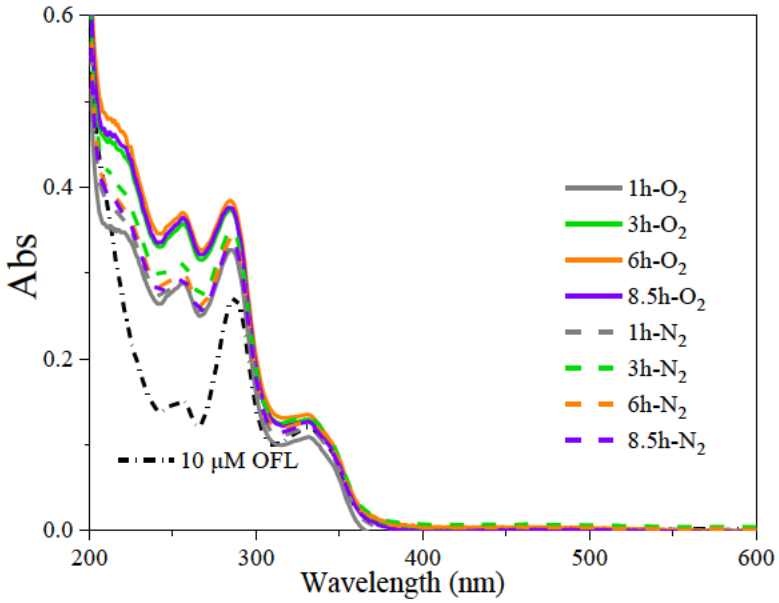

Figure S9. UV-Vis spectra during reaction under anoxic and oxic conditions at pH 8 (± 0.1). 345 µM acid birnessite;10 µM OFL;10 mM NaCl; 200 µM Mn(II); 1 mM sodium pyrophosphate.

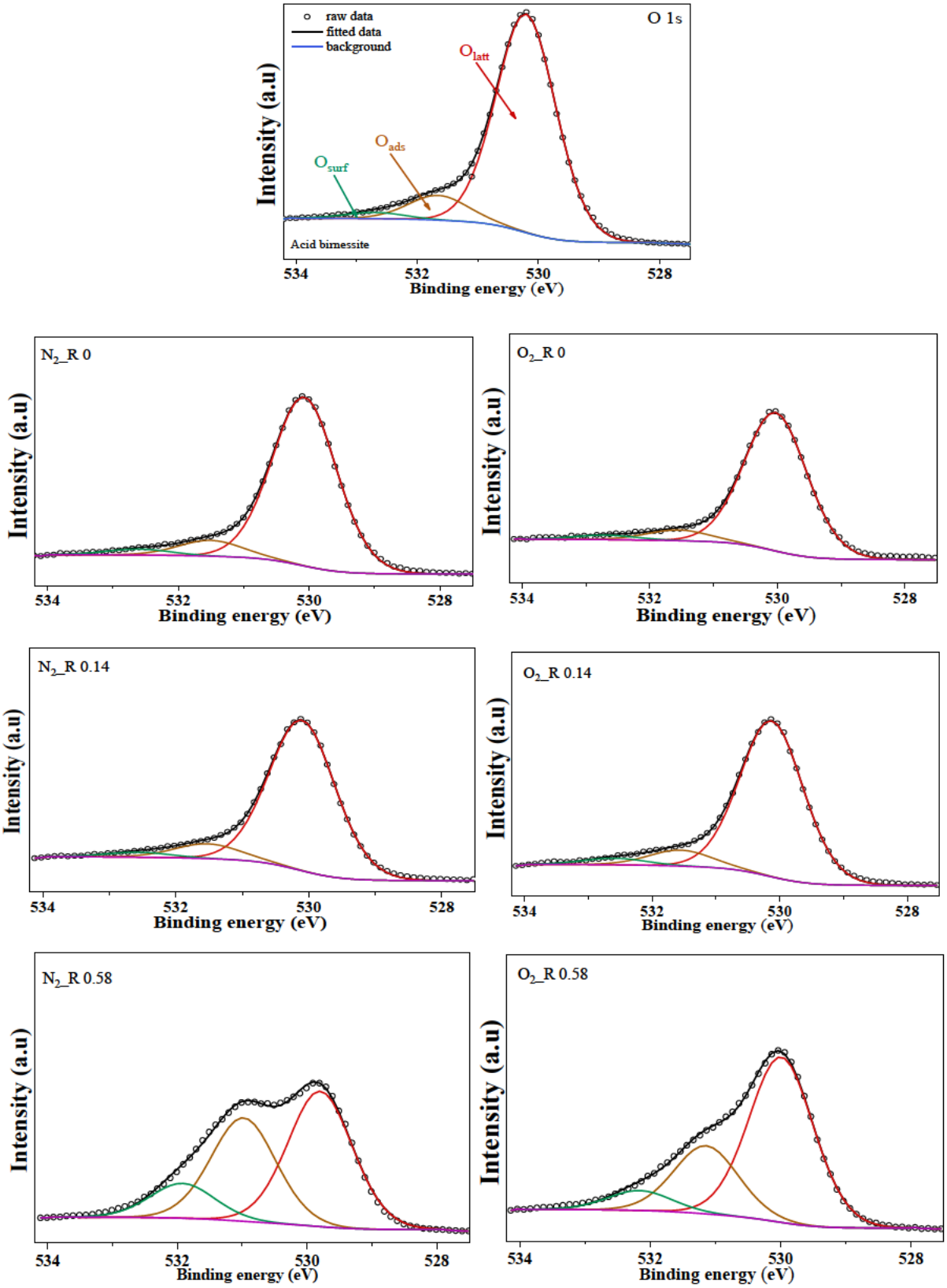

Figure S10. Fitting of O 1s XPS high resolution spectra of pristine MnO_2 and samples treated with Mn(II) and OFL under oxic and anoxic condition. The R represents the Mn(II)/MnO_2 molar ratio. 345 µM acid birnessite; 10 µM OFL; 10 mM NaCl; 0, 50, 200 µM Mn(II); 48 h reaction time; pH 8 (±0.1).

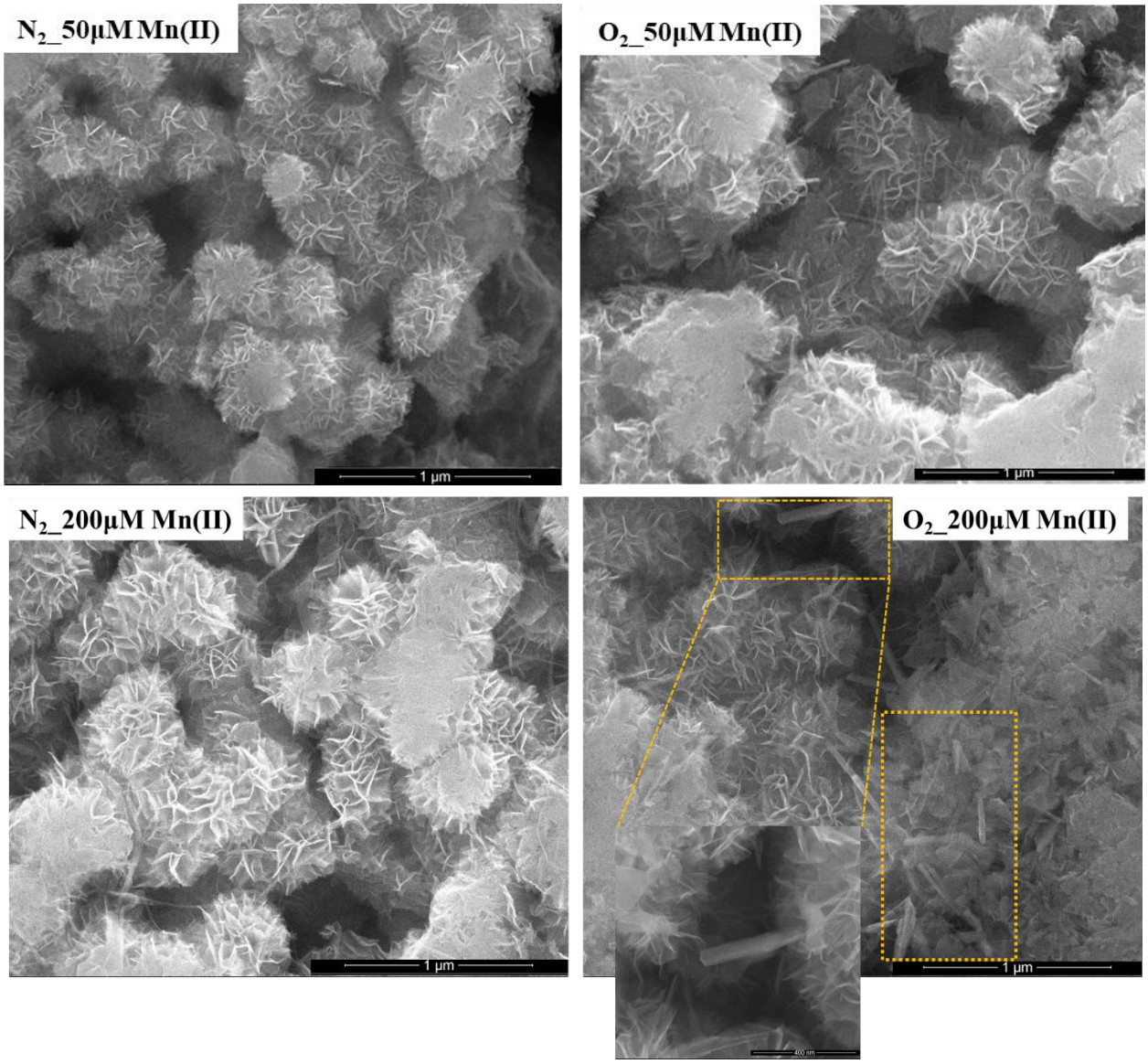

Figure S11. SEM images for samples after reaction with OFL and different Mn(II) concentrations. 345 µM acid birnessite; 10 µM OFL; 10 mM NaCl; 50, 200 µM Mn(II); 48 h reaction time; pH 8 (±0.1).

References

Zhang, H., Huang, C., 2005. Oxidative Transformation of Fluoroquinolone Antibacterial Agents and Structurally Related Amines by Manganese Oxide. Environ. Sci. Technol. 39, 4474-4483.